Journal of Sedimentary Research

Journal of Sedimentary Research, 2020, v. 90, 673–686
Research Article
DOI: http://dx.doi.org/10.2110/jsr.2020.36

THE STRATIGRAPHIC EVOLUTION OF A SUBMARINE CHANNEL: LINKING SEAFLOOR DYNAMICS TO DEPOSITIONAL PRODUCTS

STEPHEN M. HUBBARD,[1] ZANE R. JOBE,[2] BRIAN W. ROMANS,[3] JACOB A. COVAULT,[4] ZOLTAN SYLVESTER,[4] AND ANDREA FILDANI[5]

[1]*Department of Geoscience, University of Calgary, Calgary, Alberta T2N 1N4, Canada*
[2]*Department of Geology and Geological Engineering, Colorado School of Mines, Golden, Colorado 80401, U.S.A.*
[3]*Department of Geosciences, Virginia Tech, Blacksburg, Virginia 24061, U.S.A.*
[4]*Bureau of Economic Geology, Jackson School of Geosciences, University of Texas at Austin, Texas 78713, U.S.A.*
[5]*The Deep Time Institute, P.O. Box 27552, Austin, Texas 78755-7552, U.S.A.*

ABSTRACT: **We investigate the relationship between the cross-sectional geomorphic expression of a submarine channel as observed on the seafloor and the stratigraphic product of long-lived erosion, bypass, and sediment deposition. Specifically, by reconstructing the time–space evolution of an individual channel fill (i.e., channel element) exposed in outcrop, we establish a genetic link between thick-bedded channel-element-axis sandstone to thinly interbedded channel-element-margin deposits. Although the bounding surface between axis sandstone and margin thin beds is sharply defined, it is composed of a series of geomorphic surface segments of various ages; as such, the composite stratigraphic surface (~ 17 m relief) was formed from numerous incision events that repeatedly sculpted the conduit. By demonstrating the origin of the stratigraphic surface, we conclude that geomorphic surfaces with 2–7 m of erosional relief were largely responsible for the observed intra-channel-element architecture (and ultimately, the composite 17-m-thick element). The widely documented channel element axis-to-margin architecture is a product of submarine-channel thalweg dynamics, primarily recording interactions between the seafloor and the basal high-concentration layers of channelized turbidity currents.**

INTRODUCTION

Submarine channel systems are important conveyors of sediment, nutrients, and pollutants from continents to deep-sea basins (Piper and Normark 2001; Liu et al. 2013; Kane and Clare 2019). They are carved by gravity-driven density currents, and their sedimentary fills contain a record of protracted sediment transfer across slopes (Deptuck et al. 2003; Hubbard et al. 2014; Englert et al. 2020). The inaccessibility of the deep sea and the large magnitude of sediment-laden currents that shape submarine channels, however, make formative processes difficult to observe (Bouma et al. 1985; Normark et al. 1993; Talling et al. 2015). Recent efforts to: 1) directly monitor flows in channels (e.g., Paull et al. 2010; Xu et al. 2013; Hughes Clarke 2016; Azpiroz-Zabala et al. 2017); 2) record seascape morphodynamics via repeat bathymetric surveys (e.g., Conway et al. 2012; Hughes Clarke et al. 2015; Hage et al. 2018); and 3) interpret high-resolution seafloor data (Maier et al. 2011; Jobe et al. 2015, 2017; Carvajal et al. 2017), have provided new insights that inspire re-evaluation of traditional datasets, including the stratigraphic record.

Mutti and Normark (1987) integrated observations from three-dimensional seafloor mapping with cross sections of channel fills from outcrop to reconcile the definition of a submarine channel as an elongated depression on the seafloor actively traversed by flows. Outcrop studies have shown that channel-filling strata can exhibit a variety of facies and architectures, from amalgamated sandstone beds interpreted to have been deposited from high-density turbidity currents (cf. Lowe 1982) to more heterolithic thin-bedded successions above channel floors often attributed to deposition from lower-density tails of turbidity currents (e.g., Walker 1975; Barton et al. 2010; Hubbard et al. 2014; Stevenson et al. 2015). Until very recently, what can be observed in outcrop (i.e., sedimentary fill of a single channel) was below the resolution of bathymetric data (Maier et al. 2011; Conway et al. 2012; Jobe et al. 2015; Carvajal et al. 2017).

Channel-form-shaped sedimentary bodies, or channel fills, are common in the stratigraphic record, at multiple scales and associated with a breadth of depositional settings. Experimental (e.g., Sheets et al. 2007; de Leeuw et al. 2018b), modeling (e.g., Strong and Paola 2008; Sylvester et al. 2011), seismic interpretation (e.g., Deptuck et al. 2003), and outcrop (e.g., Reimchen et al. 2016) studies have shown that the basal surfaces of channel fills are commonly composite and often highly time transgressive (Fig 1). Outcrops of deposits of sandstone-dominated submarine channel fills occur in a variety of basin settings through Earth history. Although their facies and stratigraphic architecture can be highly variable (Wynn et al. 2007), they are commonly characterized by beds that bidirectionally lap onto confining erosion surfaces (Fig. 1A; Mutti and Normark 1987; Beaubouef et al. 1999; Sullivan et al. 2000; Gardner et al. 2003; McHargue et al. 2011; Fildani et al. 2013; Macauley and Hubbard 2013; Li et al. 2016; Jimenez et al. 2018; Casciano et al. 2019). Large-scale channel-fill bounding surfaces in the deep-water stratigraphic record are likely to form through deep incision, mass wasting, or migration and aggradation of a smaller geomorphic channel-form template (e.g., Sylvester et al. 2011; Gamberi et al. 2013; Bain and Hubbard 2016; Hodgson et al. 2016). These

Published Online: July 2020
Copyright © 2020, SEPM (Society for Sedimentary Geology) 1527-1404/20/090-673

Downloaded from http://pubs.geoscienceworld.org/sepm/jsedres/article-pdf/90/7/673/5129451/i1527-1404-90-7-673.pdf
by guest

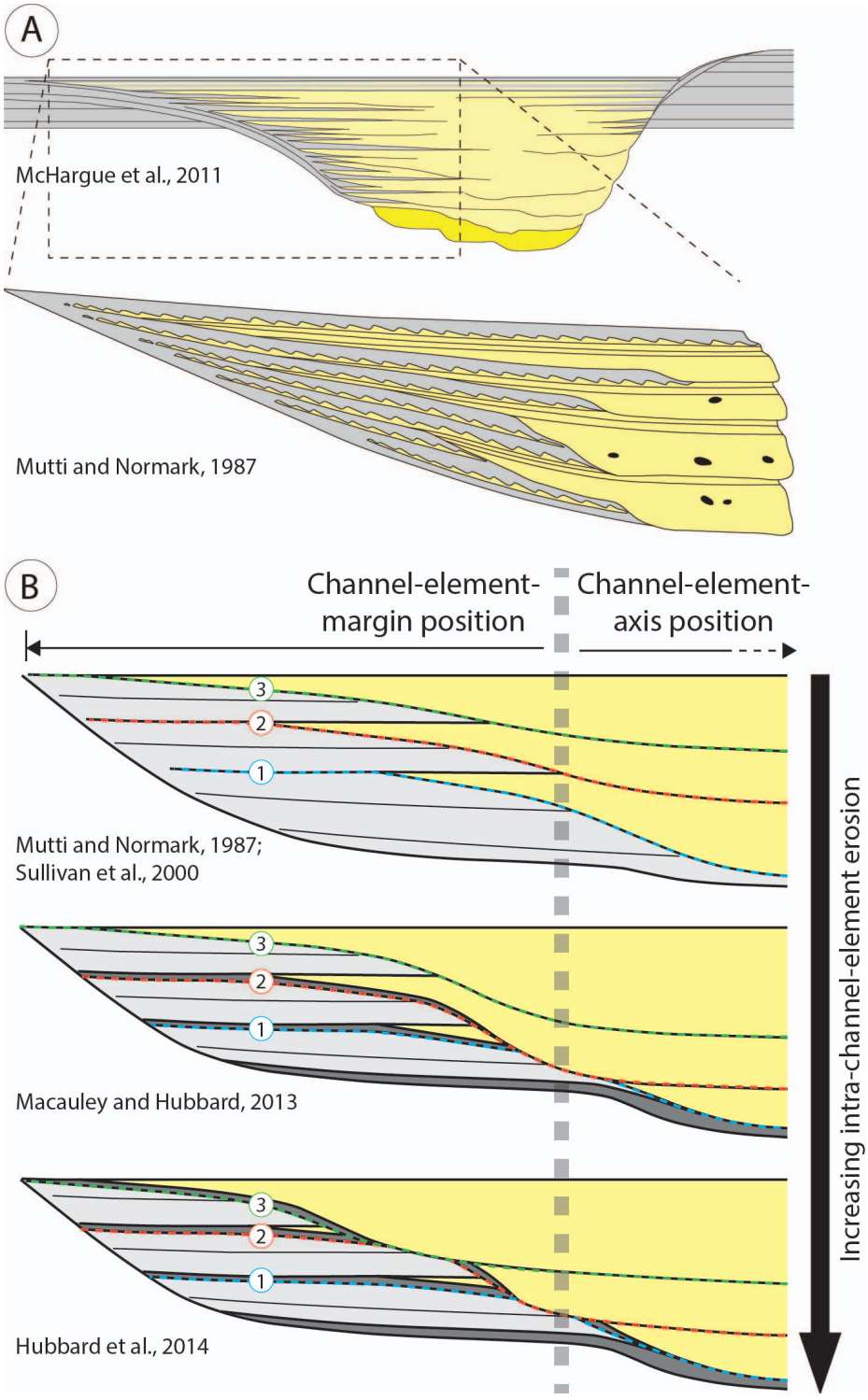

FIG. 1.—Channel-element stratigraphic architecture. **A)** Channel elements highlighting the basal erosion surface overlain by a fill that includes numerous erosion surfaces (modified from Mutti and Normark 1987; McHargue et al. 2011). Coarse-grained amalgamated sandstone beds transition laterally to thinner bedded sandstone and siltstone. **B)** Half channel widths that show variable configurations of internal erosion surfaces (i.e., secondary channel-form surfaces labeled 1–3), largely differentiated by depth of incision. The degree of incision controls the nature of interfingering amongst siltstone and thick-bedded sandstone at the transition between the element axis and margin. Approximate scales of sketches are 15–25 m thick (maximum) and 100–200 m wide.

fundamental observations and interpretations have been critical for developing realistic perspectives of long-term channel evolution on deep-water slopes (e.g., Englert et al. 2020).

The primary objective of this study is to reconstruct the time–space evolution of stratigraphic surfaces in the sedimentary fill of a single submarine channel in the Upper Cretaceous Tres Pasos Formation, southern Chile. In doing so, we demonstrate the diachronous development of key surfaces traceable in an outcropping channel fill, highlighting: 1) the polyphase history of erosion, sediment bypass, and deposition; and 2) the linkages between the geomorphic expression of the channel at any one time and the resultant time-averaged stratigraphic product. The characterization of diachronous stratigraphic surfaces provide insight into refined evolutionary models of long-term sediment transfer, as well as the minimum number of flows necessary to form and maintain an active conduit on the seafloor.

Downloaded from http://pubs.geoscienceworld.org/sepm/jsedres/article-pdf/90/7/673/5129451/i1527-1404-90-7-673.pdf
by guest

SUBMARINE CHANNEL ELEMENTS

The analysis of submarine channel-fill units has been widely couched in the context of stratigraphic hierarchy (Pickering et al. 1995; Sprague et al. 2002; Mayall et al. 2006; McHargue et al. 2011; Cullis et al. 2018). These classification schemes have proven useful for delineation and comparison of deep-water hydrocarbon reservoirs (McHargue et al. 2011), and we aim to explore aspects of their morphodynamic origins. In these schemes, the channel fill (Sprague et al. 2002) or channel element (McHargue et al. 2011) is the largest order composed of repeated, or even predictable, internal facies architecture (Fig. 1). This entails thick-bedded, amalgamated sandstone deposited in the interpreted paleo-thalweg (i.e., channel-element axis), and thinly interbedded sandstone and mudstone at channel margins (Mutti and Normark 1987). Overall, a more complete record of channel evolution is preserved in channel-margin deposits compared to channel-axis deposits, which has been attributed to higher energy and erosive processes (i.e., net erosion, low deposition) typical in channel thalwegs (Conway et al. 2012; Hubbard et al. 2014; Covault et al. 2016). Hubbard et al. (2014) described the element-bounding surface as a "primary channel-form surface."

Hubbard et al. (2014) developed an evolutionary model of protracted phases of erosion, sediment bypass, and deposition to account for the widely observed characteristics of intra-channel-element architecture. They emphasized the importance of 3–5-m-thick channel-form sandstone bodies, which collectively stack to compose a channel element. These intra-element features have been observed in outcrops globally, and have been commonly termed "channel stories" (e.g., Campion et al. 2005; Pyles et al. 2010; Li et al. 2016); the bounding surfaces of intra-element channel-forms have been also described as "secondary channel-form surfaces" (Hubbard et al. 2014). While a channel story represents the sedimentary fill between two intra-channel-fill erosion surfaces, it is important to note that they are contained in the larger channel element. Because they are regularly documented only in 2D, strike-oriented cross sections cannot be reliably correlated down-dip for greater than hundreds of meters in most instances, it is plausible that they represent either localized scours or more continuous channelized features (e.g., Mitchell 2006; Fildani et al. 2013; Gales et al. 2019; Heijnen et al. 2020). The stratigraphic expression of these features is variable and inferred to be controlled by the nature, magnitude, and frequency of erosive events that partially reshape the conduit (Fig. 1B), as well as the geomorphic asymmetry of the formative channel (Fig 1A; McHargue et al. 2011; Reimchen et al. 2016; Shumaker et al. 2018).

METHODOLOGY AND STUDY AREA

The study area is in the Magallanes retroarc foreland basin of southern Chile in the vicinity of Laguna Figueroa, $\sim$ 40 km north of the town of Puerto Natales (Fig. 2). The outcrop belt features a Campanian-age deep-water slope segment located 25–30 km down-dip (southward) from coeval paleo-shelf deposits, and the relief from paleo-shelf to the Laguna Figueora area is approximately 1000 m (Bauer et al. 2020; Fig. 2). Regional mapping of channel elements by Hubbard et al. (2010), Macauley and Hubbard (2013), Pemberton et al. (2016), and Daniels et al. (2018) has resulted in the identification of a particularly well-exposed channel element for analysis in this study, named the "M2 channel element."

The M2 channel element is 400 m wide and up to 17 m thick (Fig. 2C), the orientation of which is constrained, in part, by paleoflow measurements (mean 127°) from sole marks, the edges of scours, and the foresets of cross-beds and ripple laminae. An 80-m-long-strike-oriented transect across the left bank was selected for analysis, and characterized with a series of 17 closely spaced (4–5 m apart) measured stratigraphic sections. These sections were measured at one-millimeter resolution (82.5 m total) in order to catalogue a near complete record of sedimentation units (gravity-flow event beds; Ghosh and Lowe 1993; Hickson and Lowe 2002), from thick-bedded sandstone in a channel-element-axis position to thinly interbedded sandstone and mudstone in a channel-element margin position. Measured sections were correlated with an emphasis on secondary channel-form surfaces. Channel deposits in the Tres Pasos Formation are widely observed to onlap and/or drape element-defining erosion surfaces (Hubbard et al. 2014), although this onlap surface (i.e., primary channel-form surface) is not exposed in the studied outcrop due to vegetative cover (Fig. 2D).

RESULTS

Sedimentation Units and Facies

Thick-bedded, amalgamated turbidites (Facies 1) comprise sandstone-dominated packages up to 15 m thick (Figs. 3A, 4). Individual sedimentation units range in thickness from 0.5 to 145 cm, and locally contain mudstone intraclasts overlying the basal contact. The sandstone deposits are often apparently structureless, attributed to the collapse of high-density turbidity currents (Lowe 1982) (Fig. 3A). However, diffuse subhorizontal or wavy stratification is common (Fig. 3B). Cross-stratification is locally preserved, and is interpreted to be caused by bedload transport of medium- to coarse-grained sand (Lowe 1982; Postma et al. 2014).

Thin- to thick-bedded, non-amalgamated turbidites (Facies 2) characterize heterolithic packages up to 5.5 m thick (Fig. 3C). Event beds are 0.2–95 cm thick and are commonly characterized by the low-density turbidite divisions of Bouma (1962) (Fig. 3D–F). Bioturbation is moderately abundant in these deposits, particularly in muddy turbidite caps; ichnogenera present include *Ophiomorpha*, *Palaeophycus*, *Phycosiphon*, *Planolites*, *Scolicia*, and *Skolithos* (Hubbard et al. 2012).

Sedimentation units composed primarily of mudstone that overlie sharply defined erosion surfaces are also present (Facies 3) (Fig. 3G). In some cases, these beds contain a medium- to coarse-grained basal division $<$ 5 cm thick, and collectively, mudstone-dominated packages of Facies 3 are 0.1–1 m thick (Fig. 3H). Individual sedimentation units range from 0.2 to 27 cm thick. These bed types are attributed to: 1) deposition from largely bypassing currents, composed either of mud from the upper part or tails of otherwise bypassing turbidity flows or of thin lag deposits (Mutti and Normark 1987; Grecula et al. 2003; Stevenson et al. 2015); or 2) underfit turbidity flows that only deposited sand in the channel axis (Hubbard et al. 2014; Li et al. 2016).

Chaotically bedded mudstone (Facies 4) is rarely preserved in the strata studied, and where observed is closely associated with Facies 3 (Fig. 3I). Deposits are attributed to mass-wasting processes, and consist of either small-scale slump deposits or an amalgam of mudstone intraclasts.

Distribution of Sedimentation Units

The southwest extent of the outcrop (sections 1–2; Fig. 4) is dominated by amalgamated, thick sandstone beds of Facies 1. Although cliff exposures prevented directly measuring the full channel-element thickness at these locations, we used photomosaics (e.g., Fig. 2D) to confirm correlation of the top of the sandstone package to other measured sections. At sections 3–6, the base of the section consists of a mudstone-dominated unit 20–90 cm thick beneath the thick sandstone package (Fig. 4); this recessive unit is composed of chaotically bedded deposits (Facies 4) or thin, sand-poor turbidites (Facies 3) (Fig. 3H, I). We interpret that sections 1–6 occupy an axis position in the channel element, with erosion and bypass recorded by Facies 3 and 4, followed by a record of collapsing, depositing turbidity currents (Facies 1). In this part of the outcrop at least 57 distinct sedimentation units are described, the majority of which are preserved in the fine-grained deposits that drape the primary channel-form surface (i.e., base of section 6; Fig. 4). These fine-grained deposits were

Downloaded from http://pubs.geoscienceworld.org/sepm/jsedres/article-pdf/90/7/673/5129451/i1527-1404-90-7-673.pdf
by guest

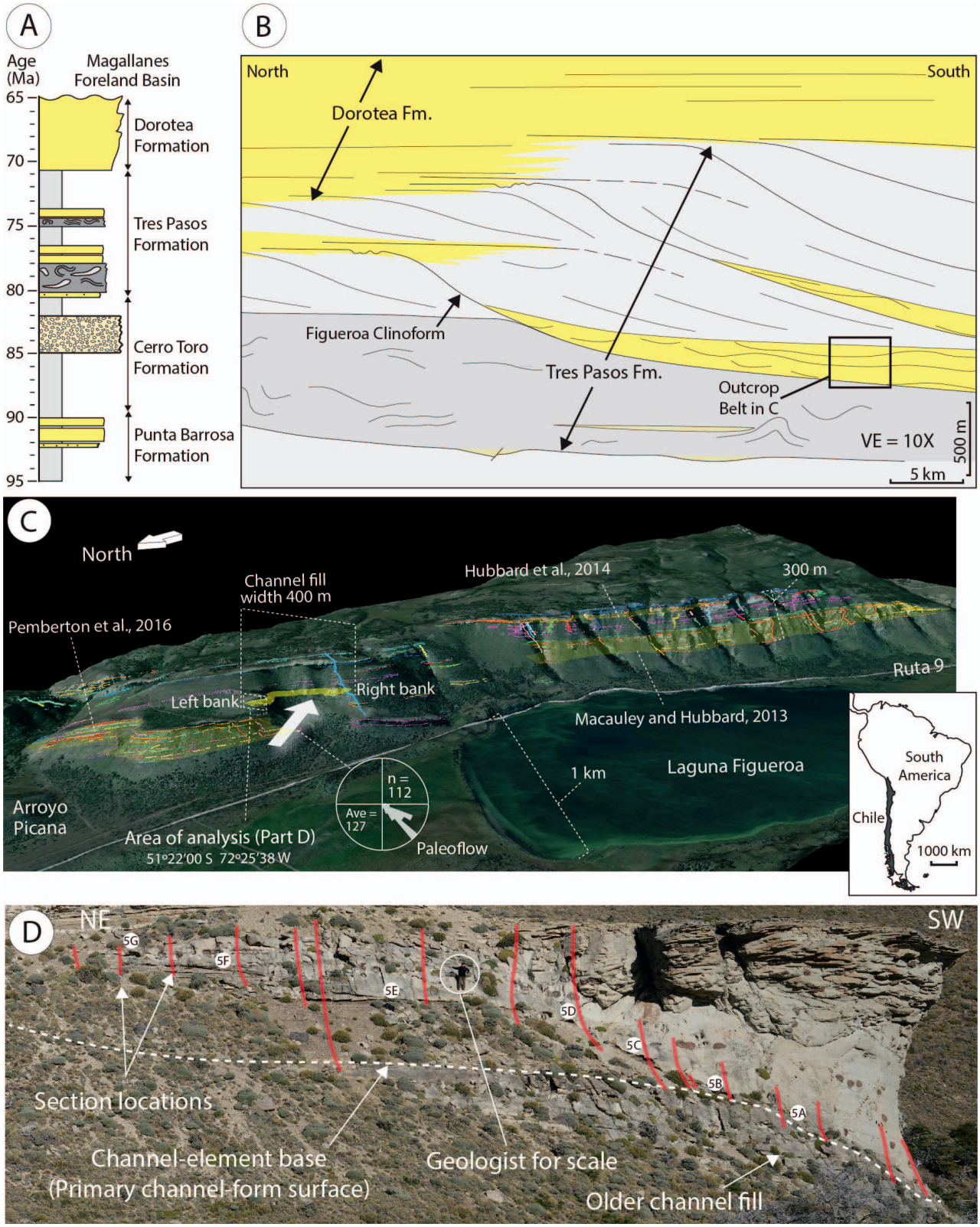

FIG. 2.—Study overview. **A)** Lithostratigraphic framework, **B)** depositional context, **C)** perspective image of outcrop belt, and **D)** detail of outcrop transect of channel element studied. Parts A and B are modified from Auchter et al. (2020) and Bauer et al. (2020). Circled labels in Part D show locations of features in figures. Satellite image data in Part C is from Google, Landsat, Copernicus 2016, http://www.google.com/earth/index.html. Digital elevation model and dataset first shown by Pemberton et al. (2016).

Downloaded from http://pubs.geoscienceworld.org/sepm/jsedres/article-pdf/90/7/673/5129451/i1527-1404-90-7-673.pdf
by guest

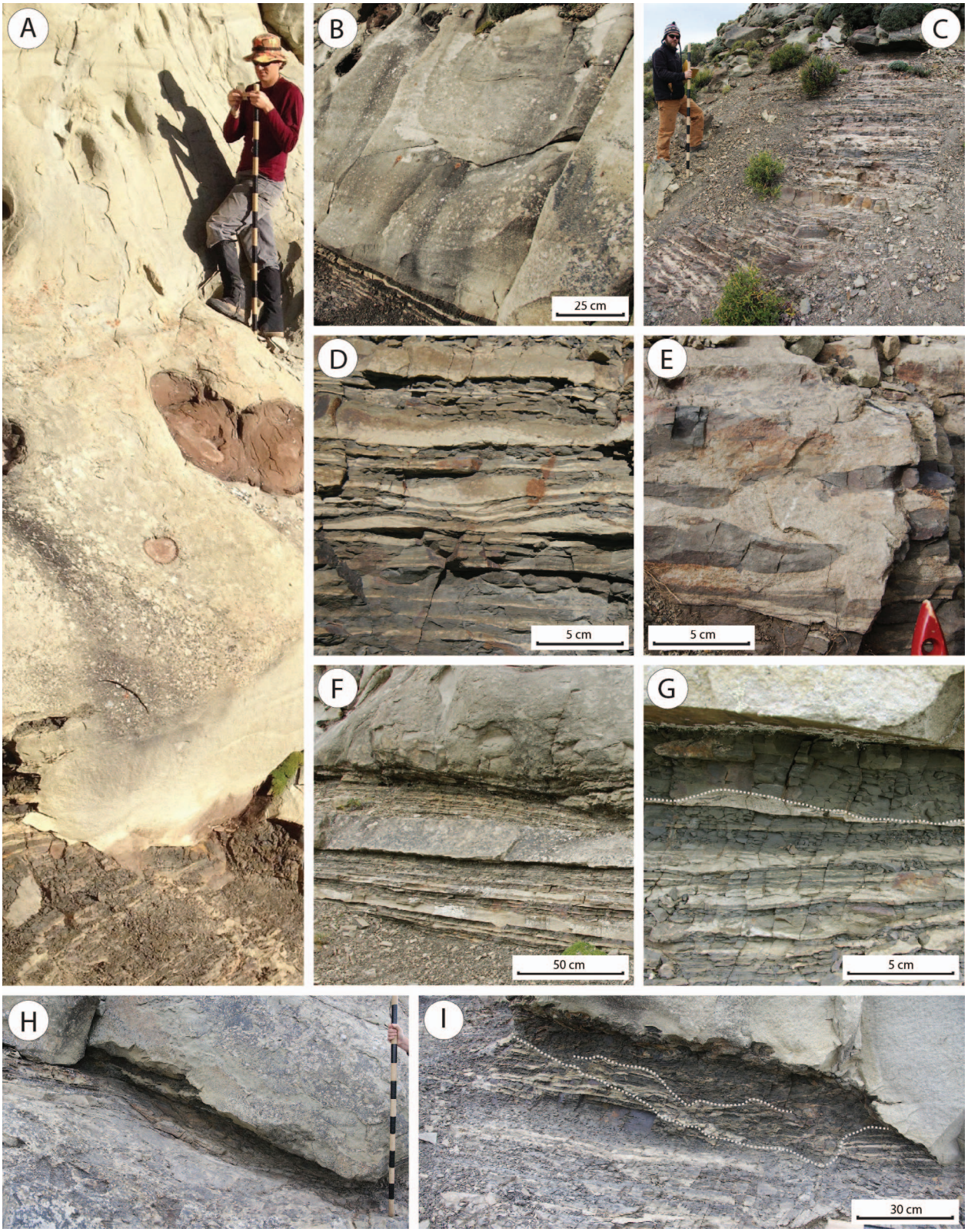

FIG. 3.—Bed-scale sedimentary characteristics of the channel element, highlighting various sedimentation-unit styles preserved in the M2 Channel outcrop. **A**, **B)** Thick-bedded sandstone of Facies 1 in measured sections 1 and 10, respectively. **C**–**F)** Thin- to thick-bedded turbidites of Facies 2 in measured sections 12 (lower), 10 (base), 9 (lower), and 14 (middle), respectively. **G**, **H)** Mudstone overlying erosion surfaces in measured sections 11 (base) and 5 (base), respectively. **I)** Chaotically bedded mudstone of Facies 4 with mudstone of Facies 3 at base of measured section 6.

Downloaded from http://pubs.geoscienceworld.org/sepm/jsedres/article-pdf/90/7/673/5129451/i1527-1404-90-7-673.pdf
by guest

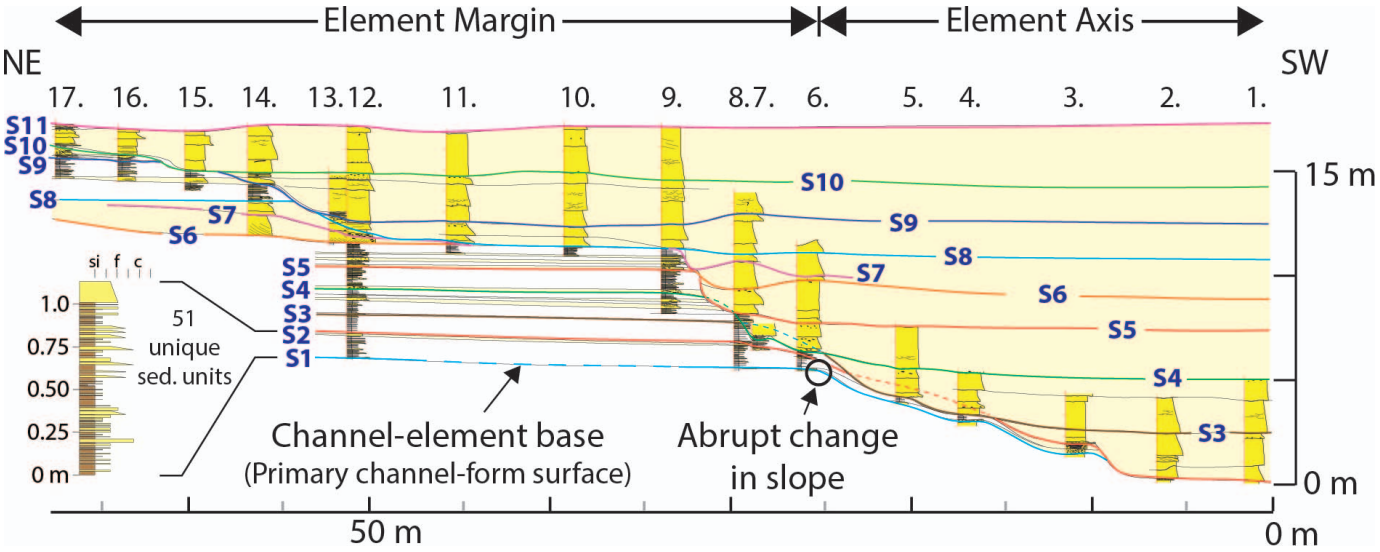

FIG. 4.—Stratigraphic cross section of the channel element axis-to-margin transition exposed in the outcrop, with measured-section locations indicated in Figure 2D. The secondary channel-form surfaces are labeled S1–S11; the primary channel-form surface includes parts of S1 and S2. Paleoflow is into the page.

removed by subsequent erosion in sections 1–5. Notably, the base of the channel element (i.e., primary channel-form surface) is characterized by an abrupt change in slope (i.e., a step or notch) at the approximate location of section 6, across which it is generally subhorizontal to the northeast (light blue line in Fig. 4).

Sections 7–9 record the sharp lateral transition from thick-bedded sandstone (Facies 1) to thin-bedded sandstone and mudstone (Facies 2) (Figs. 4, 5A, B). The abrupt lateral termination of thin beds demarks the change from the channel-element-axis position to the margin position. Thin-bedded turbidites of Facies 2 are pervasive in the northeast end of the outcrop, with 434 unique turbidite sedimentation units identified (sections 10–17; Fig. 4) in an interpreted channel-margin position. Although sedimentation units are typically $<$ 1–5 cm thick and characterized by normal grading from fine or very fine-grained sandstone to siltstone, there are rare sedimentation units 5–30 cm thick that are composed of upper medium- to coarse-grained sandstone with subangular to subrounded mudstone intraclasts (Fig. 3E). Importantly, correlation of the secondary channel-form surfaces suggests that thin beds in the lower part of the margin succession (Facies 2) are coeval to axis deposits (Facies 1) in sections 1–6 (Fig. 4).

The uppermost 4–6 m of the channel element in sections 9–17 is characterized by amalgamated sandstone (Facies 1), which transitions laterally across secondary channel-form surfaces to thin-bedded sandstone and mudstone (Facies 2) to the northeast (Figs. 4, 5C). The base of this upper section is relatively flat, and is overlain by a cross-bedded sandstone up to 90 cm thick (Figs. 4, 5D). The upward bed thickening from Facies 2 at the base to Facies 1 at the top is common to channel-element-margin sequences (Fig. 1; Mutti and Normark 1987; Gardner et al. 2003; Grecula et al. 2003; Campion et al. 2005; Di Celma et al. 2011; Macauley and Hubbard 2013).

Stratigraphic Surfaces

Sedimentation units are distributed within a series of mappable packages that are defined by secondary channel-form surfaces. In the sandstone-dominated axis position, these surfaces are locally characterized by a grain-size shift from medium- to coarse-grained sandstone, mudstone intraclast lags, and/or overlying cross-beds. At the sharp (typically erosional) contact between the axis sandstone to the southwest and the thin-bedded margin strata to the northeast, distinct notches, or steps, in secondary channel-form surfaces record up to 4.5 m of relief over $<$ 2 m laterally (Figs. 4, 5A). At the element axis-to-margin facies transition, these surfaces contain evidence for incision and undulating relief: 1) sandstone beds with mudstone intraclasts (Figs. 3E, I, 5B), 2) mudstone-prone sedimentation units attributed to bypass of coarse-grained sediment (Figs. 3F, 5C, E), or 3) thin sandstone beds in the channel margin composed of sandstone of grain size similar to that observed in the channel-element axis (e.g., sections 1–6 in Fig. 4).

Direct stratigraphic correlation between channel-element axis and margin strata is challenging due to erosion and modification of the surfaces from subsequent phases of channel evolution (Figs. 1, 4). The basis for these correlations includes: 1) physical correlation at the top of the succession (e.g., surface S10; Fig. 4), where turbidity currents did not erode the surface that connects axis-to-margin units. 2) Bed thickness and grain-size trends in the margin deposits—in particular, the coarsest beds in the margin could be interpreted to reflect sediment bypass during the incision of a new secondary channel-form surface (e.g., Fig. 3E). The similarity in the maximum grain size of some margin and axis beds links the highest energy phases of sedimentation across the channel transect (Fig. 4). 3) The same number of mapped erosion surfaces are preserved in both element-axis and element-margin strata (Fig. 4). 4) The prevalence of secondary channel-form surfaces and the strata they bound (i.e., channel stories) in other channel elements at the same stratigraphic level in the Tres Pasos Formation, which are of similar scale and internal character (Fig. 2; Macauley and Hubbard 2013).

Outcrop Synthesis

The M2 channel element is characterized by a distinct, abrupt change in slope along its basal surface, with evidence for deep scour to the SW (i.e., towards the axis), and more flat-lying and higher elevation character to the NE (i.e., towards the left-hand margin) across sections 6–9 (Fig. 4). This surface records erosion to varied levels during the initial establishment of the conduit (Fildani et al. 2013). The point of abrupt change in slope of the basal surface was apparently critical to channel evolution, as it is aligned with the overlying sharply defined lateral transition from amalgamated sandstone of the channel-element-axis position to thin-bedded sandstone and siltstone of the channel-element-margin position (Fig. 4). This is

Downloaded from http://pubs.geoscienceworld.org/sepm/jsedres/article-pdf/90/7/673/5129451/i1527-1404-90-7-673.pdf
by guest

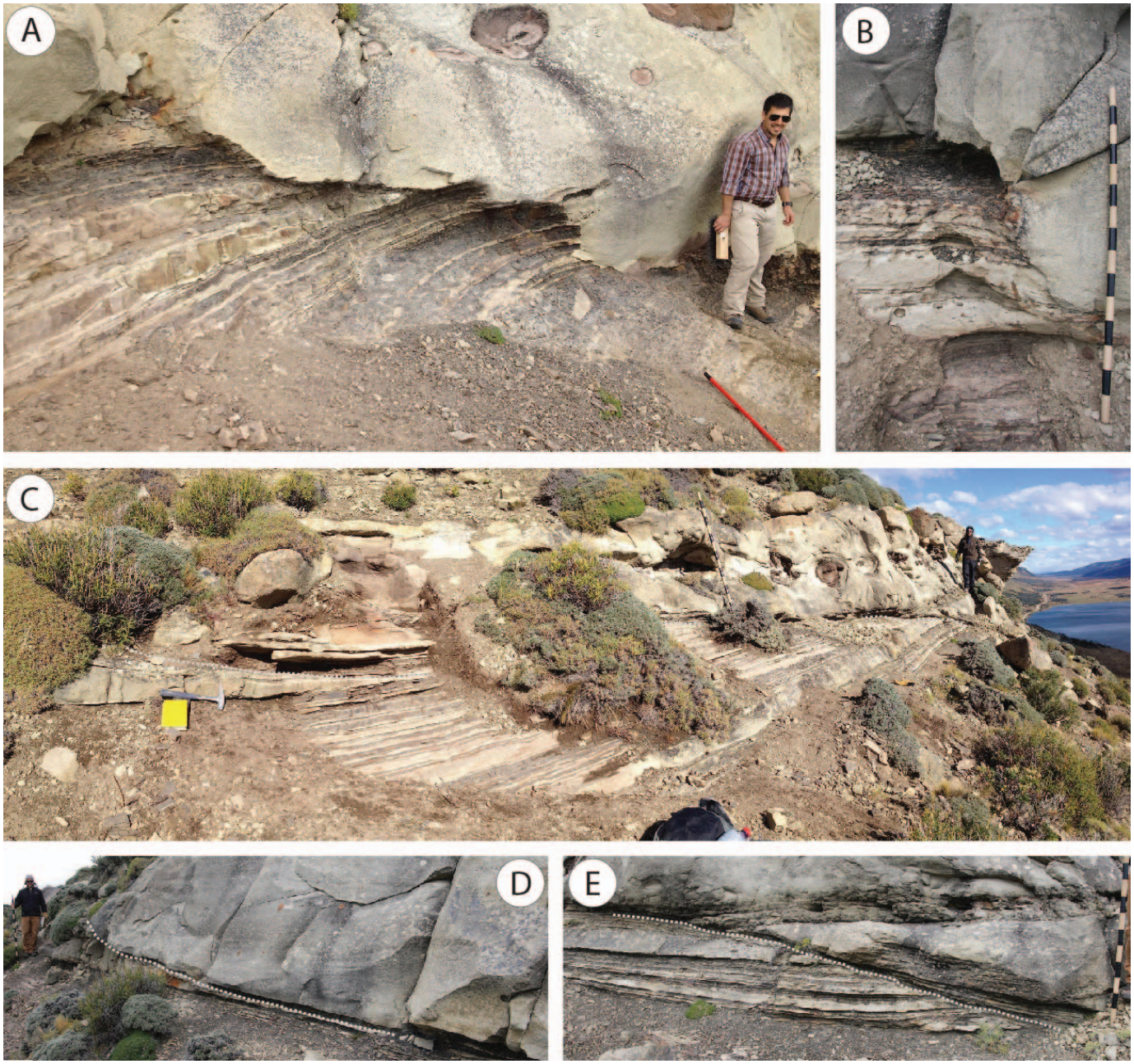

FIG. 5.—Photographs highlighting various aspects of intra-channel-element architecture. **A**, **B)** Stepped incision surface that defines the lateral boundary between thick-bedded amalgamated sandstone (Facies 1) and thick- to thin-bedded sandstone and mudstone (Facies 2). **C)** Mudstone-draped low-angle erosion surface at the northeast end of the outcrop (measured sections 16 and 17). **D**, **E)** Mudstone-draped secondary channel-form surfaces between measured sections 11 and 12. The location of each photo is indicated in Figure 2D.

consistent with observations from other submarine channel elements (e.g., Sullivan et al. 2000; Gardner et al. 2003; Hubbard et al. 2014). Although not a focus of this study, it is interesting to hypothesize that channel elements which lack the abrupt change in slope along their basal surface do not develop a well-defined channel-element-facies transition from axis-sandstone to margin-thin beds. Hubbard et al. (2014) interpreted that early flows that bypassed or deposited coarse-grained sediment in the deepest part of the channel were associated with deposition of thin sand beds in the channel margin. Effectively, the abrupt change in slope of the primary channel-form surface records initial development of a terrace (cf. Maier et al. 2012); as subsequent flows bypassed or deposited sediment in the channel thalweg, this area was the locus for deposition of thin-bedded turbidites from the upper parts of stratified flows (Hubbard et al. 2014; Hansen et al. 2015; Li et al. 2016; Jobe et al. 2017). This is consistent with many numerical and physical experiments, which have demonstrated that channel confinement through erosional processes is enhanced by aggradation at channel margins (e.g., Hall et al. 2008; Rowland et al. 2010; de Leeuw et al. 2018a).

The notched, or stepped, profile of the composite channel-element-axis sandstone body records a series of 2–7-m-thick, vertically stacked channel-form bodies (i.e., stories) bounded by secondary channel-form erosional surfaces (Figs. 1, 5). These strata record distinct phases of erosion, bypass,

Downloaded from http://pubs.geoscienceworld.org/sepm/jsedres/article-pdf/90/7/673/5129451/i1527-1404-90-7-673.pdf
by guest

and deposition during the protracted evolution of the channel (cf. Hubbard et al. 2014). Similar steps at the edges of coarse-grained channel bodies have been described in seismic, outcrop, and experimental datasets, and are attributed to the generation of composite stratigraphic surfaces through punctuated stages of channel evolution (e.g., Hubbard et al. 2008; Maier et al. 2012; de Leeuw et al. 2018a). The erosional bases of these steps are interpreted to correlate to discrete packages bounded by the erosion surfaces in the thick, heterolithic channel-element-margin succession (Figs. 1, 5).

Geomorphic data have been used to demonstrate that an individual flow can contemporaneously deposit thick-bedded (i.e., element axis) sediments in the channel thalweg and thin-bedded (i.e., element margin) sediments at a higher elevation (e.g., Normark and Reid 2003; Pirmez and Imran 2003; Jobe et al. 2017). This makes direct correlations between deposits of the two settings challenging because of postdepositional erosion, modification, and compaction. The likelihood of a direct physical correlation between element axis and margin deposits increases with decreasing scour relief.

The deposition of sand across the top of the thin-bedded margin succession, including the unique prevalence of cross stratification at the base of this sandstone succession (e.g., sections 9–11 in Fig. 4), is interpreted to reflect expansion of turbidity currents during the late-stage evolution of the conduit as relief is filled. Overall, an upwards trend towards wider and lower-relief secondary channel-form surfaces is apparent (Fig. 4), consistent with previous studies (Hubbard et al. 2014; de Leeuw et al. 2018b).

TIME–SPACE EVOLUTION OF A SUBMARINE-CHANNEL ELEMENT

To examine the time–space evolution of the M2 channel element, we construct a diagram of channel-element half-width against interpreted relative time (Fig. 6) (i.e., Wheeler diagram; Wheeler 1958, 1964). There are several important caveats about the construction of such a diagram. First, the primary value is to aid investigation of relative timing of sedimentation events and the temporal nature of composite stratigraphic surfaces based on the observed and interpreted stratigraphic architecture. Thus, it is not an independent assessment of the accuracy of that interpretation. We discriminate three temporal domains: deposition, non-deposition, and erosion/non-preservation.

Assumptions with such an analysis are inevitable, with critical assumptions including: 1) secondary channel-form surfaces (e.g., S1, S2, etc.) are interpreted to have developed over short duration, and thus, are depicted as instantaneous (i.e., flat) surfaces in the Wheeler diagram (Fig. 6). The sedimentation units are tabulated between these successive erosion surfaces. 2) Temporal positions of thick sandstone beds in the channel thalweg cannot be precisely determined due to lateral pinch-out against erosion surfaces; thus, uncertainty is shown by a vertical line with arrow heads at each end depicting the relative timing range possible for the beds (Fig. 6). 3) The events are distributed equally through time simply to show relative stacking; we do not assume or infer temporal breaks and/or temporal clustering. While we recognize that the equal distribution of beds in a unit bounded by secondary channel-form surfaces is simplistic, we have no temporal data (e.g., flow recurrence intervals) to constrain the unequal placement of beds within these packages.

Approximately 70–80% of the channel-element exposure consists of sandstone-dominated (axis) strata, and 20–30% is thinly interbedded sandstone and mudstone (margin) (Fig. 4). Stratigraphic sections measured from the channel-element axis through margin transition document the number and spatial distribution of sedimentation units. Our analysis reveals that 520 individual, distinct sedimentation units are present in the channel-element strata assessed. The total number of distinct sedimentation units represents the minimum number of turbidity currents that passed through the channel over its lifecycle. While $\sim$ 80% of the area of the exposure are channel-element-axis deposits, $<$ 10% of the recorded sedimentation units are preserved in axis deposits (Fig. 6). Particular insight into prolonged sediment transfer during channel evolution is consequently preserved not in the axis, but in cross-sectionally (and thus volumetrically) limited channel-margin sedimentation units (cf. Hubbard et al. 2014). These observations complement recent depositional-system-scale interrogation of stratigraphic completeness, which emphasize the use of gaps in the stratigraphic record to inform paleoenvironmental interpretations (Trabucho-Alexandre 2014; Mahon et al. 2015; Durkin et al. 2018; Vendettuoli et al. 2019).

Correlation of secondary channel-form surfaces reveals that thinner-bedded, finer-grained channel element margin facies are coeval with thicker-bedded axis facies (Fig. 4). An interpretation of time-transgressive channel evolution is required to account for these observations (Fig. 7). A simplistic, two-step, cut-and-fill model (Beaubouef et al. 1999; Camacho et al. 2002; Kolla et al. 2012) does not represent the prolonged and dynamic nature of evolutionary processes that resulted in the composite and diachronous nature of the erosional surface that bounds channel-element-axis sandstone. Thick-bedded, sand-rich, sediment gravity flows that deposited in the channel thalweg were episodic, or even rare ($<$ 10% of flows), against a background of channel maintenance by bypassing and erosive turbidity currents (Covault et al. 2014). Moreover, repeated deep-incision events also limit the preservation potential of the thick-bedded element-axis deposits by removing their sedimentary record (cf. Vendettuoli et al. 2019). During the evolution of the channel, incision events repeatedly sculpted the bank, with interpreted relief between the thalweg and margin between 2.5 m and 6.5 m (Fig. 7B–K). In contrast, relief estimated from the edge of the composite sandstone body is 17.4 m (Fig. 7L). The disparity in these values underscores the importance of recognizing the stratigraphic expression of channel evolution (cf. Fig. 1B). Despite the smooth appearance of the surface that defines the edge of sandstone-dominated channel-element-axis strata, this surface never existed on the seafloor, but rather was formed over a protracted period and is composed of a series of geomorphic surface segments of various ages that variably coalesce and diverge (Fig. 7L). Further, the Wheeler analysis demonstrates the origin of upward bed-thickening patterns in channel-element margins (Grecula et al. 2003; Macauley and Hubbard 2003), reflecting the decrease in channel relief through time (Fig. 7).

Onlap of thick sandstone beds against low-relief secondary channel-form surfaces, as well as repeated deposition of thin, coarse-grained sandstone beds in the channel margin, can be reconciled with flows characterized by distinct flow stratification (Middleton 1993; Sumner and Paull 2014; Jobe et al. 2017; Symons et al. 2017). The banks of lower-relief ($<$ 8 m) channel surfaces are overcome by the basal coarse-sand rich parts of flows much more readily than in instances where a deep incision ($>$ 15 m) is present. Recognition that secondary channel-form surfaces in a channel element record the evolution of the geomorphic channel has important implications for interpretation of formative flow properties and morphodynamics from the stratigraphic record. For example, the characteristic channel depth is thought to be scaled to the high-density basal parts of turbidity currents that pass through channels (Pirmez and Imran 2003).

The stratified nature of channelized turbidity currents has been widely discussed (e.g., Middleton 1993), and recently documented from direct monitoring (Xu et al. 2014; Hughes Clarke 2016; Azpiroz-Zabala et al. 2017; Stevenson et al. 2018), seafloor core-sampling (Jobe et al. 2017; Symons et al. 2017), experiments (e.g., Cartigny et al. 2014; de Leeuw et al. 2018a), and numerical modeling studies (Abd El-Gawad et al. 2012; Bolla Pittaluga and Imran 2014; Eggenhuisen et al. 2017; Luchi et al. 2018; Traer et al. 2018). These studies all indicate that sand is commonly confined to the basal part of the flow, and thus primarily deposited in or near the channel thalweg in many instances. Numerous recent outcrop analyses have considered the impact of flow stratification on facies relationships observed in submarine channel fills (e.g., Arnott 2007; Dykstra and Kneller 2009; Hansen et al. 2015). In particular, the typically

Downloaded from http://pubs.geoscienceworld.org/sepm/jsedres/article-pdf/90/7/673/5129451/i1527-1404-90-7-673.pdf
by guest

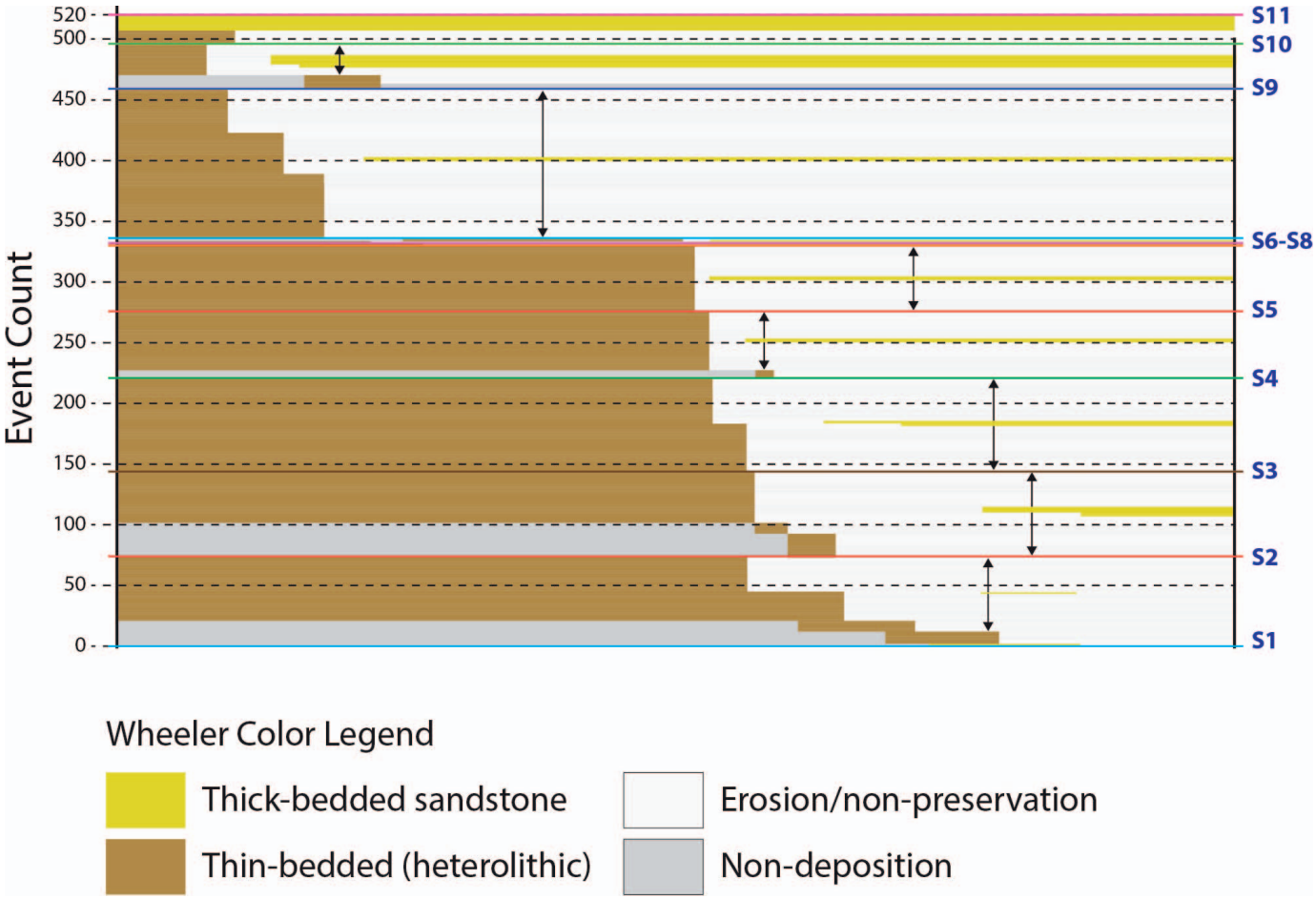

FIG. 6.—Wheeler-diagram interpretation of the channel element investigated. The horizontal axis corresponds to the lateral extent of the stratigraphic cross-section in Figure 4. The vertical axis reflects the number of distinct sedimentation units counted in each of the measured sections along the outcrop transect, with each event bed spaced equally regardless of deposit thickness. The secondary channel-form erosional surfaces described in the outcrop belt are labelled S1–S11.

limited ability of flows to spill coarse-grained sediment into channel-margin settings is reflected by the sharp lateral facies transitions between channel-axis and channel-margin deposits (Hubbard et al. 2014). In submarine channels offshore Nigeria, Jobe et al. (2017) demonstrated coeval deposition in channel-axis and channel-margin settings, and even modest elevation changes (~ 10 m) across channel cross-sectional profiles were associated with significant differences in grain size, event-bed thickness, and facies.

In the Tres Pasos Formation, the: 1) relief of mapped secondary channel-form surfaces, and 2) coarsest sandstone beds that can be tracked between thalweg and margin, provide thickness estimates of 2–7 m for the basal, high sediment concentration layers within the stratified turbidity currents as the beds observed were deposited. This estimate of the basal high-concentration layer compares to recent observations from direct monitoring studies (Sumner and Paull 2014; Azpiroz-Zabala et al. 2017), numerical modeling (Eggenhuisen et al. 2017), and seafloor core studies (Jobe et al. 2017), supporting the interpretation of the M2 channel element of the Tres Pasos Formation (Fig. 7).

DISCUSSION

Temporal Scales of Composite Channel Surface Generation

The formation of stratigraphic surfaces through various stages of erosion and sedimentation in channelized settings is well established (e.g., Holbrook 2001; Deptuck et al. 2003; Törnqvist et al. 2003; Hodgson et al. 2016). Strong and Paola (2008) constructed a particularly insightful experiment that demonstrated the development of a highly diachronous incised-valley bounding surface through numerous deepening and widening episodes during various developmental stages. Sylvester et al. (2011) suggested that the idea of the fundamental difference between geomorphic and stratigraphic surfaces also applies to submarine channel systems. The implications for interpretation of the stratigraphic record are significant, and specifically that stratigraphically defined valley or channel shapes often do not represent a former geomorphic (i.e., topographic) surface. In submarine channel settings, substantial aggradation driven by constructional overbank sedimentation can lead to formation of a valley-scale stratigraphic surface that could be misleading and suggest a single phase of deep incision, followed by protracted infill (cf. Deptuck et al. 2003; Sylvester et al. 2011; Bain and Hubbard 2016; Hodgson et al. 2016). Various studies have shown that these stratigraphic surfaces could be generated by multiple flows over thousands (e.g., Jobe et al. 2015) to millions (e.g., Englert et al. 2020) of years.

Recent outcrop-based studies have examined the generation of stratigraphic surfaces through coalescing of geomorphic surface segments at a finer scale and over much shorter time periods. Durkin et al. (2015) analyzed fluvial point-bar strata and interpreted diachronous stratigraphic surfaces that were variably sculpted by erosion or modified through sedimentation around a point-bar reach through changing river stages.

Downloaded from http://pubs.geoscienceworld.org/sepm/jsedres/article-pdf/90/7/673/5129451/i1527-1404-90-7-673.pdf
by guest

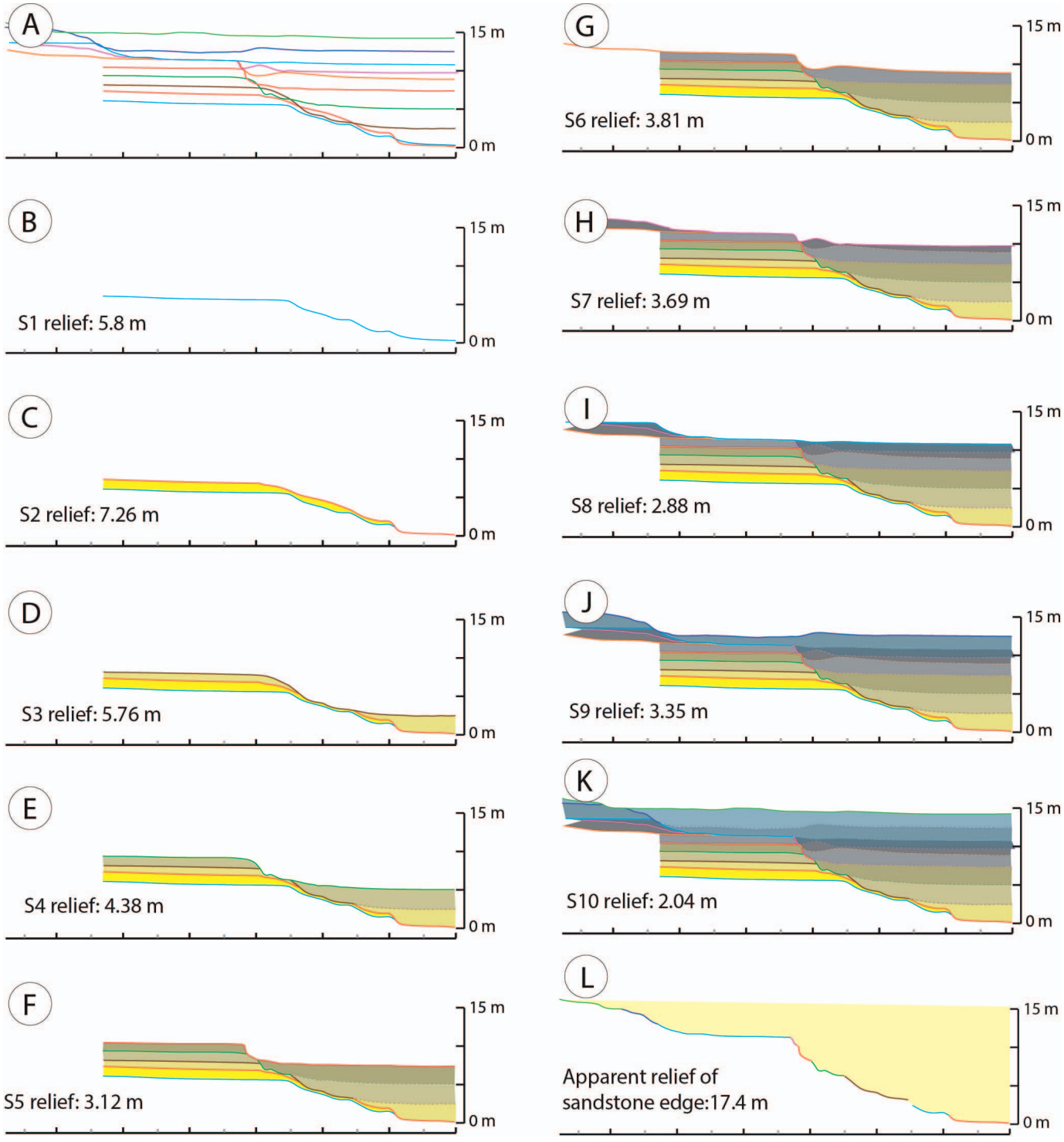

FIG. 7.—Geomorphic-surface evolution and the generation of the stratigraphic surface that defines the edge of the sandstone-dominated channel-element-axis sedimentary body. Part L shows that the edge of the sandstone (i.e., the stratigraphic surface) is defined by eight geomorphic surface segments from evolutionary stages presented in B–K. Fill color gradation records time steps from oldest deposits (lighter, yellow) to younger deposits (darker, gray).

Although these surfaces may have been shaped over a short duration (e.g., seasonal river cycle), like the experimental stratigraphic-surface-defined valleys of Strong and Paola (2008), they never corresponded to a geomorphic surface that once existed in the meander belt. Reimchen et al. (2016) compared the primary channel-form surfaces that define deep-water channel elements to channel surfaces on the seafloor, noting a 16% discrepancy in the normalized cross-sectional areas of the channel-fill sedimentary bodies and geomorphic channels. They attributed the larger cross-sectional area of sedimentary bodies in the rock record to protracted erosion and sedimentation processes, which sculpted the diachronous

Downloaded from http://pubs.geoscienceworld.org/sepm/jsedres/article-pdf/90/7/673/5129451/i1527-1404-90-7-673.pdf
by guest

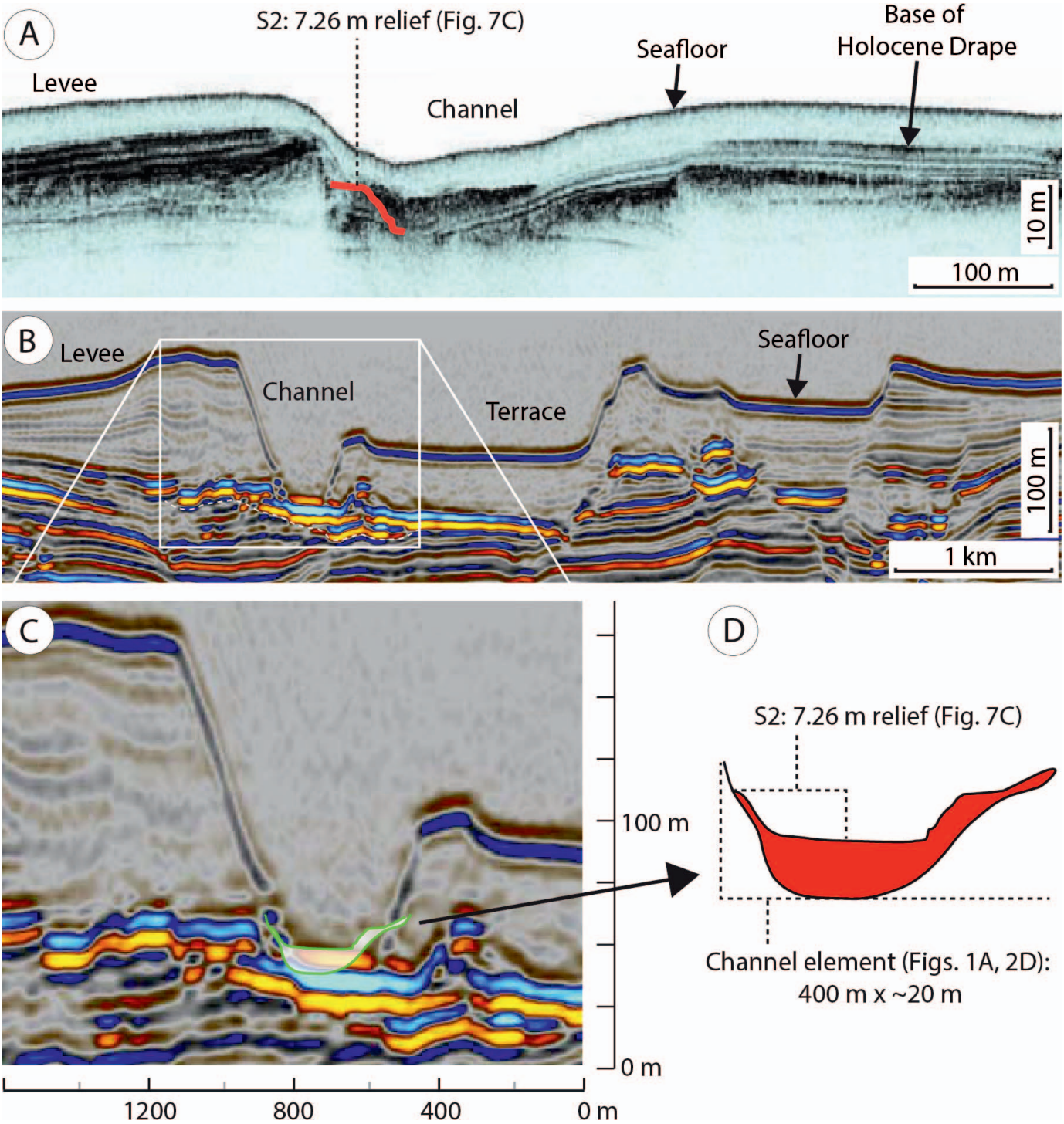

FIG. 8.—Comparison of the Tres Pasos Formation outcrop-derived surfaces with **A)** seafloor and near-seafloor data from Lucia Chica (Maier et al. 2011, 2012)—a scaled secondary erosion surface is overlaid on a comparable surface in the chirp data (2–15 Kz profile with 10 cm resolution). **B)** Seafloor and shallow seismic profile (50 Hz data) from Hansen et al. (2017) (Seismic dataset owner: PGS). Despite the fact that the channel on the seafloor is > 1 km wide, the thalweg (defined by bright amplitude) is the same scale as the outcrop channel element (D).

stratigraphic surface over an extended period (e.g., Sheets et al. 2007; Gamberi et al. 2013; Pemberton et al. 2016). Our analysis builds on previous work, outlining the role of intra-channel surfaces (i.e., secondary channel-form surfaces) and the strata that they bound (i.e., channel stories) in the overall evolution of submarine channels.

The recognition of a diachronous lateral contact (Fig. 7L) between the sandstone-dominated channel element axis and adjacent thin-bedded element margin in the Tres Pasos Formation has potentially wide-ranging implications. Importantly, the submarine-channel-fill style described is widely observed in outcrop and subsurface datasets from numerous basin

Downloaded from http://pubs.geoscienceworld.org/sepm/jsedres/article-pdf/90/7/673/5129451/i1527-1404-90-7-673.pdf
by guest

settings around the world (e.g., Mutti and Normark 1987; Sullivan et al. 2000; Gardner et al. 2003; Grecula et al. 2003; Mayall et al. 2006; McHargue et al. 2011; Macauley and Hubbard 2013; Bain and Hubbard 2016; Li et al. 2016). In many instances, the > 17-m-thick composite sandstone-rich body (Fig. 7L; channel element axis) would have historically been considered for estimating paleo-hydraulic conditions on the ancient slope. However, the geomorphic surface likely never had that much relief—it evidently formed due to the protracted aggradation of a smaller channel-form-shaped geomorphic template (Fig. 7). It is this template, defined by secondary channel-form surfaces in the outcrop, which records sculpting and deposition by turbidity currents. We suggest that this template might be most useful for reconstructing formative turbidity-current properties, including sediment discharge and concentration (e.g., Azoiroz-Zabala et al. 2017; de Leeuw et al. 2018b; Li et al. 2018; Stevenson et al. 2018).

Linking Outcrops to Seafloor Observations

The challenge of linking the stratigraphic record to observations of deep-water seafloor geomorphology has been widely discussed over the last three decades (e.g., Bouma et al. 1985; Normark et al. 1993; Gamberi et al. 2013). Initially, it was recognized that the scales of investigation were disparate amongst methodological approaches, with seafloor remote-sensing techniques enabling coarse-scale observations relative to outcrops (Bouma et al. 1985; Mutti and Normark 1987; Clark and Pickering 1996). Remote-sensing tools, such as seismic-reflection data, have improved since the 1980s; however, despite significant developments in data processing, resolution limits are demonstrated to result in a composite seismic expression that masks the fine-scale geometric and stratigraphic details that might enable insight into formative sedimentary processes (Normark et al. 1993; Abreu et al. 2003; Bakke et al. 2008; Pemberton et al. 2018). Recently, high-resolution bathymetric data integrated with very high-resolution (up to 0.25 m vertical resolution) seismic reflection or core data have provided unprecedented perspectives of the seafloor and underlying deposits (e.g., Maier et al. 2011; Carvajal et al. 2017; Hage et al. 2018). These data resolve outcrop-scale features, enabling a fruitful re-evaluation of the linkage between the surfaces and deposits observed in various datasets.

We posit that the secondary channel-form surfaces with 2–7 m relief (Fig. 7), and the collective ~ 17-m-thick, sand-rich channel element that formed through their protracted aggradation (Fig. 4), are likely associated with the basal part of levee-bounded submarine channel systems that are widely observed on the modern seafloor (Fig. 8). These deposits are primarily influenced only by the basal, highest-density parts of thick, stratified flows (Pirmez and Imran 2003; Arnott 2007). This could help explain the dimension disparity between channels on the seafloor and outcropping channel fills. Fine-grained terraces, overbank, and eventually levees add appreciable depth to active channels, but with limited preservation (or exposure) potential and compaction significantly influencing diagnostic geometries, they are often poorly exposed or difficult to reconstruct in outcrops (e.g., Macauley and Hubbard 2013). This has undoubtedly made linkage between outcrops and modern channel systems particularly difficult, especially with regard to development of holistic process-to-product models for submarine channel systems (Mutti and Normark 1987; Wynn et al. 2007; Gamberi et al. 2013). The stratigraphic channel element axis-to-margin facies transition captures channel thalweg dynamics, and should be readily distinguished from coeval, much finer and thinner-bedded inner levee or levee units.

CONCLUSIONS

Reconstructing the time-space evolution of an individual deep-water channel element that crops out in southern Chile demonstrates the polyphase history of erosion, sediment bypass, and deposition that shapes submarine channel systems. The most striking initial observation of the outcrop is a sharply defined surface, which demarcates the edge and base of a sandstone-dominated channel-form body (17.4 m thick). Our fine-scale analysis demonstrates that this stratigraphic surface is composed of a series of geomorphic surface segments of various ages; as such, this composite surface formed over numerous incision events that repeatedly sculpted the setting. These various incision events were associated with 2–7 m of erosional relief, indicating that morphodynamics associated with a relatively small geomorphic template was responsible for the observed intra-channel-element architecture. This contrasts a perhaps more intuitive initial interpretation, which is that the measured relief at the edge of the channel-axis sandstone (i.e., 17.4 m) corresponds to the geomorphic relief that would have existed on the seafloor. From our analysis, we posit that the channel-element fill pattern examined, consisting of channel-axis sandstone transitioning laterally to thinly-interbedded channel margin deposits over short distances, is a product of submarine-channel thalweg dynamics, primarily recording interactions between the seafloor and the basal high concentration layers of channelized turbidity currents.

ACKNOWLEDGMENTS

This research was graciously supported by sponsors of the Chile Slope Systems Joint Industry Project Phases 1–2 (Anadarko, BG Group, BHP Billiton, BP, Chevron, CNOOC, ConocoPhillips, Equinor, Hess, Marathon, Repsol, and Shell). Discussions with scientists from various sponsors have significantly impacted our understanding of slope channel systems. Sebastian Kaempfe, Ben Daniels, and Aaron Reimchen assisted with the fieldwork. Bret Dixon, Morgan Sullivan, and an anonymous reviewer provided helpful input for which we are particularly grateful.

REFERENCES

Abd El-Gawad, S.M., Pirmez, C., Cantelli, A., Minisini, D., Sylvester, Z., and Imran, J., 2012, 3-D numerical simulation of turbidity currents in submarine canyons off the Niger Delta: Marine Geology, v. 326–328, p. 55–66, doi: 10.1016/j.margeo.2012.06.003.

Abreu, V., Sullivan, M., Pirmez, C., and Mohrig, D., 2003. Lateral accretion packages (LAPs): an important reservoir element in deep water sinuous channels: Marine and Petroleum Geology, v. 20, p. 631–648.

Arnott, R.W.C., 2007, Stratal architecture and origin of lateral accretion deposits (LADs) and conterminous inner-bank levee deposits in a base-of-slope sinuous channel, lower Isaac Formation (Neoproterozoic), East-Central British Columbia, Canada: Marine and Petroleum Geology, v. 24, p. 515–528.

Auchter, N.C., Romans, B.W., Hubbard, S.M., Daniels, B.G., Scher, H.D., and Buckley, W., 2020, Intrabasinal sediment recycling from detrital strontium isotope stratigraphy: Geology, v. 48, doi: 10.1130/G47594.1.

Azpiroz-Zabala, M., Cartigny, M.J.B., Talling, P.J., Parsons, D.R., Sumner, E.J., Clare, M.A., Simmons, S.M., Cooper, C., and Pope, E.L., 2017, Newly recognized turbidity current structure can explain prolonged flushing of submarine canyons: Science Advances, v. 3, e1700200.

Bain, H.A., and Hubbard, S.M., 2016, Stratigraphic evolution of a long-lived submarine channel system in the Late Cretaceous Nanaimo Group, British Columbia, Canada: Sedimentary Geology, v. 337, p. 113–132, doi: 10.1016/j.sedgeo.2016.03.010.

Bakke, K., Gjelberg, J., and Petersen, S.A., 2008, Compound seismic modelling of the Ainsa turbidite system, Spain: application to deep-water channel systems offshore Angola: Marine and Petroleum Geology, v. 25, p. 1058–1073.

Barton, M., O'Byrne, C., Pirmez, C., Prather, B., van der Vlugt, F., Alpak, F.O., and Sylvester, Z., 2010, Turbidite channel architecture: recognizing and quantifying the distribution of channel base drapes using core and dipmeter data, *in* Pöppelreiter, M., Garcia-Carballido, C., and Kraaijveld, M.A., eds., Dipmeter and Borehole Image Log Technology: American Association of Petroleum Geologists, Memoir 92, p. 195–210.

Bauer, D.B., Hubbard, S.M., Covault, J.A., and Romans, B.W., 2020, Inherited depositional control on shelf-margin oversteepening, readjustment, and coarse-grained sediment delivery to deep water, Magallanes Basin, Chile: Frontiers in Earth Science, v. 7, article 358.

Beaubouef, R.T., Rossen, C., Sullivan, M.D., Mohrig, D.C., and Jennette, D.C., 1999, Deep-water sandstones, Brushy Canyon Formation, west Texas, *in* Field Guide, American Association of Petroleum Geologists. Hedberg Field Research Conference, Continuing Education, Course Note Series 40, 47 p.

Bolla Pittaluga, M., and Imran, J., 2014, A simple model for vertical profiles of velocity and suspended sediment concentration in straight and curved submarine channels: Journal of Geophysical Research, Earth Surface, v. 119, p. 483–503.

Downloaded from http://pubs.geoscienceworld.org/sepm/jsedres/article-pdf/90/7/673/5129451/i1527-1404-90-7-673.pdf
by guest

Bouma, A.H., 1962, Sedimentology of Some Flysch Deposits: A Graphic Approach to Facies Interpretation: Amsterdam, Elsevier, 168 p.

Bouma, A.H., Normark, W.R., and Barnes, N.E., 1985, COMFAN: needs and initial results, *in* Bouma, A.H., Normark, W.R., and Barnes, N.E., eds., Submarine Fans and Related Turbidite Systems: New York, Springer, Frontiers in Sedimentology, p. 7–11.

Camacho, H., Busby, C.J., and Kneller, B., 2002, A new depositional model for the classical turbidite locality at San Clemente State Beach, California: American Association of Petroleum Geologists, Bulletin, v. 86, p. 1543–1560.

Campion, K.M., Sprague, A.R., and Sullivan, M.D., 2005, Architecture and lithofacies of the Capistrano Formation (Miocene–Pliocene), San Clemente, California: American Association of Petroleum Geologists, Pacific Section, Fieldtrip Guidebook 100, 42 p.

Cartigny, M.J.B., Ventra, D., Postma, G., and van Den Berg, J.H., 2014, Morphodynamics and sedimentary structures of bedforms under supercritical-flow conditions: new insights from flume experiments: Sedimentology, v. 61, p. 712–748, doi: 10.1111/sed.12076.

Carvajal, C., Paull, C.K., Caress, D.W., Fildani, A., Lundsten, E., Anderson, K., Maier, K.L., McGann, M., Gwiazda, R., and Herguera, J.C., 2017, Unraveling the channel–lobe transition zone with high resolution AUV bathymetry: Navy Fan, offshore Baja California, Mexico: Journal of Sedimentary Research, v. 87, p. 1049–1059.

Casciano, C.I., Patacci, M., Longhitano, S.G., Tropeano, M., McCaffrey, W.D., and Di Celma, C., 2019, Multi-scale analysis of a migrating submarine channel system in a tectonically-confined basin: the Miocene Gorgoglione Flysch Formation, southern Italy: Sedimentology, v. 66, p. 205–240.

Clark, J.D., and Pickering, K.T., 1996, Architectural elements and growth patterns of submarine channels: application to hydrocarbon exploration: American Association of Petroleum Geologists, Bulletin, v. 80, p. 194–220.

Conway, K.W., Vaughn Barrie, J., Picard, K., and Bornhold, B.D., 2012, Submarine channel evolution: active channels in fjords, British Columbia, Canada: Geo-Marine Letters, v. 32, p. 301–312.

Covault, J.A., Kostic, S., Paull, C.K., Ryan, H.F., and Fildani, A., 2014, Submarine channel initiation, filling and maintenance from sea-floor geomorphology and morphodynamic modeling of cyclic steps: Sedimentology, v. 61, p. 1031–1054.

Covault, J.A., Sylvester, Z., Hubbard, S.M., Jobe, Z.R., and Sech, R.P., 2016, The stratigraphic record of submarine-channel evolution: SEPM, The Sedimentary Record, v. 14, n. 3, p. 4–11.

Cullis, S., Colombera, L., Patacci, M., and McCaffrey, W.D., 2018, Hierarchical classifications of the sedimentary architecture of deep-marine depositional systems: Earth-Science Reviews, v. 179, p. 38–71.

Daniels, B.G., Auchter, N.C., Hubbard, S.M., Romans, B.W., Matthews, W.A., and Stright, L., 2018, Timing of deep-water slope evolution constrained by large-n detrital and volcanic ash zircon geochronology, Cretaceous Magallanes Basin, Chile: Geological Society of America, Bulletin, v. 130, p. 438–454.

De Leeuw, J., Eggenhuisen, J.T., and Cartigny, M.J.B., 2018a, Linking submarine channel–levee facies and architecture to flow structure of turbidity currents: insights from flume tank experiments: Sedimentology, v. 65, p. 931–951.

De Leeuw, J., Eggenhuisen, J.T., Spychala, Y.T., Heijnen, M.S., Pohl, F., and Cartigny, M.J.B., 2018b, Sediment volume and grain-size partitioning between submarine channel–levee systems and lobes: an experimental study: Journal of Sedimentary Research, v. 88, p. 777–794.

Deptuck, M.E., Steffens, G.S., Barton, M., and Pirmez, C., 2003, Architecture and evolution of upper fan channel-belts on the Niger Delta slope and in the Arabian Sea: Marine and Petroleum Geology, v. 20, p. 649–676.

Di Celma, C.N., Brunt, R.L., Hodgson, D.M., Flint, S.S., and Kavanagh, J.P., 2011, Spatial and temporal evolution of a Permian submarine slope channel–levee system, Karoo Basin, South Africa: Journal of Sedimentary Research, v. 81, p. 579–599.

Durkin, P.R., Hubbard, S.M., Boyd, R.L., and Leckie, D.A., 2015, Stratigraphic expression of intra-point-bar erosion and rotation: Journal of Sedimentary Research, v. 85, p. 1238–1257.

Durkin, P.R., Hubbard, S.M., Holbrook, J., and Boyd, R., 2018, Evolution of fluvial meander-belt deposits and implications for the completeness of the stratigraphic record: Geological Society of America, Bulletin, v. 130, p. 721–739.

Dykstra, M., and Kneller, B., 2009, Lateral accretion in a deep-marine channel complex: implications for channelized flow processes in turbidity currents: Sedimentology, v. 56, p. 1411–1432.

Eggenhuisen, J.T., Cartigny, M.J.B., and de Leeuw, J., 2017, Physical theory for near-bed turbulent particle suspension capacity: Earth Surface Dynamics, v. 5, p. 269–281, doi: 10.5194/esurf-5-269-2017.

Englert, R.G., Hubbard, S.M., Matthews, W.A., Coutts, D.S., and Covault, J.A., 2020, The evolution of submarine slope-channel systems: timing of incision, bypass, and aggradation in Late Cretaceous Nanaimo Group channel-system strata, British Columbia, Canada: Geosphere, doi: 10.1130/GES02091.1.

Fildani, A., Hubbard, S.M., Covault, J.A., Maier, K.L., Romans, B.W., Traer, M., and Rowland, J.C., 2013, Erosion at inception of deep-sea channels: Marine and Petroleum Geology, v. 41, p. 48–61.

Gales, J.A., Talling, P.J., Cartigny, M.J.B., Hughes Clarke, J., Lintern, G., Stacey, C., and Clare, M.A., 2019, What controls submarine channel development and the morphology of deltas entering deep-water fjords?: Earth Surface Processes and Landforms, v. 44, p. 535–551.

Gamberi, F., Rovere, M., Dykstra, M., Kane, I.A., and Kneller, B.C., 2013, Integrating modern seafloor and outcrop data in the analysis of slope channel architecture and fill: Marine and Petroleum Geology, v. 41, p. 83–103.

Gardner, M.H., Borer, J.M., Melick, J.J., Mavilla, N., Dechesne, M., and Wagerle, R.N., 2003, Stratigraphic process–response model for submarine channels and related features from studies of Permian Brushy Canyon outcrops, West Texas: Marine and Petroleum Geology, v. 20, p. 757–787.

Ghosh, B., and Lowe, D.R., 1993, The architecture of deep-water channel complexes, Cretaceous Vanado Sandstone Member, Sacramento Valley, California, *in* Graham, S.A., and Lowe, D.R., eds., Advances in the Sedimentary Geology of the Great Valley Group, Sacramento Valley, California: SEPM, Pacific Section, Guidebook 73, p. 51–65.

Grecula, M., Flint, S.S., Wickens, H., and Johnson, S.D., 2003, Upward-thickening patterns and lateral continuity of Permian sand-rich turbidite channel fills, Laingsburg Karoo, South Africa: Sedimentology, v. 50, p. 831–853.

Hage, S., Cartigny, M.J.B., Clare, M.A., Sumner, E.J., Vendettuoli, D., Clarke, J.E.H., Hubbard, S.M., Talling, P.J., Gwyn Lintern, D., Stacey, C.D., Englert, R.G., Vardy, M.E., Hunt, J.E., Yokokawa, M., et al., 2018, How to recognize crescentic bedforms formed by supercritical turbidity currents in the geologic record: insights from active submarine channels: Geology, v. 46, p. 563–566.

Hall, B., Meiburg, E., and Kneller, B., 2008, Channel formation by turbidity currents: Navier-Stokes based linear stability analysis: Journal of Fluid Mechanics, v. 615, p. 185–210.

Hansen, L.A.S., Callow, R.H.T., Kane, I.A., Gamberi, F., Rovere, M., Cronin, B.T., and Kneller, B.C., 2015, Genesis and character of thin-bedded turbidites associated with submarine channels: Marine and Petroleum Geology, v. 67, p. 852–879.

Hansen, L., Janocko, M., Kane, I., and Kneller, B., 2017, Submarine channel evolution, terrace development, and preservation of intra-channel thin-bedded turbidites: Mahin and Avon channels, offshore Nigeria: Marine Geology, v. 383, p. 146–167.

Heijnen, M.S., Clare, M.A., Cartigny, M.J.B., Talling, P.J., Hage, S., Lintern, D.G., Stacey, C., Parsons, D.R., Simmons, S.M., Chen, Y., Sumner, E.J., Dix, J.K., and Hughes Clarke, J.E., 2020, Rapidly-migrating and internally-generated knickpoints can control submarine channel evolution: Nature Communications, v. 11, article 3129, doi: 10.1038/s41467-020-16861-x.

Hickson, T.A., and Lowe, D.R., 2002, Facies architecture of a submarine fan channel–levee complex: the Juniper Ridge Conglomerate, Coalinga, California: Sedimentology, v. 49, p. 335–362.

Hodgson, D.M., Kane, I.A., Flint, S.S., Brunt, R.L., and Ortiz-Karpf, A., 2016, Time-transgressive confinement on the slope and the progradation of basin-floor fans: implications for the sequence stratigraphy of deep-water deposits: Journal of Sedimentary Research, v. 86, p. 73–86, doi: 10.2110/jsr.2016.3.

Holbrook, J., 2001, Origin, genetic interrelationships, and stratigraphy over the continuum of fluvial channel-form bounding surfaces: an illustration from middle Cretaceous strata, southeastern Colorado: Sedimentary Geology, v. 144, p. 179–222.

Hubbard, S.M., Romans, B.W., and Graham, S.A., 2008, Deep-water foreland basin deposits of the Cerro Toro Formation, Magallanes Basin, Chile: architectural elements of a sinuous basin axial channel belt: Sedimentology, v. 55, p. 1333–1359.

Hubbard, S.M., Fildani, A., Romans, B.W., Covault, J.A., and McHargue, T.R., 2010, High-relief slope clinoform development: insights from outcrop, Magallanes Basin, Chile: Journal of Sedimentary Research, v. 80, p. 357–375.

Hubbard, S.M., MacEachern, J.A., and Bann, K.L., 2012, Slopes, *in* Knaust, D., and Bromley, R.G., eds., Trace Fossils as Indicators of Sedimentary Environments: Amsterdam, Elsevier, Developments in Sedimentology 64, p. 607–642.

Hubbard, S.M., Covault, J.A., Fildani, A., and Romans, B.R., 2014, Sediment transfer and deposition in slope channels: deciphering the record of enigmatic deep-sea processes from outcrop: Geological Society of America, Bulletin, v. 126, p. 857–871.

Hughes Clarke, J., 2016, First wide-angle view of channelized turbidity currents links migrating cyclic steps to flow characteristics: Nature Communications, v. 7, 11896.

Hughes Clarke, J., Conway, K., Talling, P., Cartigny, M., Lintern, G., and Hill, P., 2015, Monitoring the evolution of submarine channels on fjord prodeltas and associated depositional basins: American Association of Petroleum Geologists, Search and Discovery Article 41678.

Jimenez, R.L., Cronin, B.T., Celik, H., Turner, C.C., Bastidas, R.E., and Kneller, B.C., 2018, The Alikayasi canyon-channel system (Miocene, southeast Turkey) compared with the South Brae fan system (Upper Jurassic, North Sea): characterizing sand and gravel-filled channel complexes in coarse-grained deep-water systems without gravel cone geometries, *in* Turner, C.C., and Cronin, B.T., eds., Rift-Related Coarse-Grained Submarine Fan Reservoirs: The Brae Play, South Viking Graben, North Sea: American Association of Petroleum Geologists, Memoir 115, p. 595–617.

Jobe, Z.R., Sylvester, Z., Parker, A.O., Howes, N., Slowey, N., and Pirmez, C., 2015, Rapid adjustment of submarine channel architecture to changes in sediment supply: Journal of Sedimentary Research, v. 85, p. 729–753.

Jobe, Z.R., Sylvester, Z., Pittaluga, M.B., Frascati, A., Pirmez, C., Minisini, D., Howes, N.C., and Cantelli, A., 2017, Facies architecture of submarine channel deposits on the western Niger Delta slope: implications for grain-size and density stratification in turbidity currents: Journal of Geophysical Research: Earth Surface, v. 122, p. 473–491.

Kane, I.A., and Clare, M.A., 2019, Dispersion, accumulation and the ultimate fate of microplastics in deep-marine environments: a review and future directions: Frontiers in Earth Science, doi: 10.3389/feart.2019.00080.

Downloaded from http://pubs.geoscienceworld.org/sepm/jsedres/article-pdf/90/7/673/5129451/i1527-1404-90-7-673.pdf
by guest

Kolla, V., Bandyopadhyay, A., Gupta, P., Mukherjee, B., and Ramana, D., 2012, Morphology and internal structure of a recent Upper Bengal Fan–Valley Complex, *in* Prather, B.E., Deptuck, M.E., Mohrig, D., Van Hoorn, B., and Wynn, R.B., eds., Application of the Principles of Seismic Geomorphology to Continental Slope and Base-of-Slope Systems: Case Studies from Seafloor and Near-Seafloor Analogues: SEPM, Special Publication 9, p. 145–161.

Li, L., Gong, C., and Steel, R.J., 2018, Bankfull discharge as a key control on submarine channel morphology and architecture: case study from the Rio Muni Basin, West Africa: Marine Geology, v. 401, p. 66–80.

Li, P., Kneller, B.C., Hansen, and Kane, I.A., 2016, The classical turbidite outcrop at San Clemente, California revisited: an example of sandy submarine channels with asymmetric facies architecture: Sedimentary Geology, v. 346, p. 1–16.

Liu, J.T., Kao, S.J., Huh, C.A., and Hung, C.C., 2013, Gravity flows associated with flood events and carbon burial: Taiwan as instructional source area: Annual Review of Marine Science, v. 5, p. 47–68.

Lowe, D.R., 1982, Sediment gravity flows: II. Depositional models with special reference to the deposits of high-density turbidity currents: Journal of Sedimentary Petrology, v. 52, p. 279–297.

Luchi, R., Balachandar, S., Seminara, G., and Parker, G., 2018, Turbidity currents with equilibrium basal driving layers: a mechanism for long runout: Geophysical Research Letters, v. 45, p. 1518–1526.

Macauley, R.V., and Hubbard, S.M., 2013, Slope channel sedimentary processes and stratigraphic stacking, Cretaceous Tres Pasos Formation slope system, Chilean Patagonia: Marine and Petroleum Geology, v. 41, p. 146–162.

Mahon, R.C., Shaw, J.B., Barnhart, K.R., Hobley, D.E.J., and McElroy, B., 2015, Quantifying the stratigraphic completeness of delta shoreline trajectories: Journal of Geophysical Research, Earth Surface, v. 120, p. 799–817.

Maier, K.L., Fildani, A., Paull, C.K., Graham, S.A., McHargue, T., Caress, D., and McGann, M., 2011, The elusive character of discontinuous deep-water channels: new insights from Lucia Chica channel system, offshore California: Geology, v. 39, p. 327–330.

Maier, K.L., Fildani, A., McHargue, T.R., Paull, C.K., Graham, S.A., and Caress, D.W., 2012, Punctuated deep-water channel migration: high-resolution subsurface data from the Lucia Chica Channel System, offshore California, U.S.A: Journal of Sedimentary Research, v. 82, p. 1–8.

Mayall, M., Jones, E., and Casey, M., 2006, Turbidite channel reservoirs–key elements in facies prediction and effective development: Marine and Petroleum Geology, v. 23, p. 821–841.

McHargue, T., Pyrcz, M.J., Sullivan, M.D., Clark, J., Fildani, A., Romans, B.R., Covault, J.A., Levy, M., Posamentier, H., and Drinkwater, N., 2011, Architecture of turbidite channel systems on the continental slope: patterns and predictions: Marine and Petroleum Geology, v. 28, p. 728–743.

Middleton, G.V., 1993, Sediment deposition from turbidity currents: Annual Review of Earth and Planetary Sciences, v. 21, p. 89–114.

Mitchell, N.C., 2006, Morphologies of knickpoints in submarine canyons: Geological Society of America, Bulletin, v. 118, p. 589–605.

Mutti, E., and Normark, W.R., 1987, Comparing examples of modern and ancient turbidite systems: problems and concepts, *in* Leggett, J.K., and Zuffa, G.G., eds., Deep Water Clastic Deposits: Models and Case Histories: London, Graham and Trotman, p. 1–38.

Normark, W.R., and Reid, J.A., 2003, Extensive deposits on the Pacific Plate from Late Pleistocene North American glacial lake outbursts: Journal of Geology, v. 111, p. 617–637.

Normark, W.R., Posamentier, H., and Mutti, E., 1993, Turbidite systems: state of the art and future directions: Reviews of Geophysics, v. 31, p. 91–116.

Paull, C.K., Ussler, W., Caress, D.W., Lundsten, E., Covault, J.A., Maier, K.L., Xu, J.P., and Augenstein, S., 2010, Origins of large crescent-shaped bedforms within the axial channel of Monterey Canyon, offshore California: Geosphere, v. 6, p. 755–774.

Pemberton, E.A.L., Hubbard, S.M., Fildani, A., Romans, B., and Stright, L., 2016, The stratigraphic expression of decreasing confinement along a deep-water sediment routing system: outcrop example from southern Chile: Geosphere, v. 12, p. 114–134.

Pemberton, E.A.L., Stright, L., Fletcher, S., and Hubbard, S.M., 2018, The influence of stratigraphic architecture on seismic response: reflectivity modeling of outcropping deepwater channel units: Interpretation, v. 6, p. T783–T808.

Pickering, K.T., Clark, J.D., Ricchi Lucchi, F., Smith, R.D., Hiscott, R.N., and Kenyon, N.H., 1995, Architectural element analysis of turbidite systems, and selected topical problems for sand-prone deep-water systems, *in* Pickering, K.T., Hiscott, R.N., Kenyon, N.H., Ricci Lucchi, F., and Smith, R.D.A., eds., Atlas of Deep Water Environments: Architectural Style in Turbidite Systems: London, Chapman and Hall, p. 1–10.

Piper, D.J.W., and Normark, W.R., 2001, Sandy fans: from Amazon to Hueneme and beyond: American Association of Petroleum Geologists, Bulletin, v. 85, p. 1407–1438.

Pirmez, C., and Imran, J., 2003, Reconstruction of turbidity currents in Amazon Channel: Marine and Petroleum Geology, v. 20, p. 823–849.

Postma, G., Kleverlaan, K., and Cartigny, M.J.B., 2014, Recognition of cyclic steps in sandy and gravelly turbidite sequences, and consequences for the Bouma facies model: Sedimentology, v. 61, p. 2268–2290, doi: 10.1111/sed.12135.

Pyles, D.R., Jennette, D.C., Tomasso, M., Beaubouef, R.T., and Rossen, C., 2010, Concepts learned from a 3D outcrop of a sinuous slope channel complex: Beacon Channel complex, Brushy Canyon Formation, West Texas, U.S.A.: Journal of Sedimentary Research, v. 80, p. 67–96.

Reimchen, A.P., Hubbard, S.M., Stright, L., and Romans, B.W., 2016, Using sea-floor morphometrics to constrain stratigraphic models of sinuous submarine channel systems: Marine and Petroleum Geology, v. 77, p. 92–115.

Rowland, J.C., Hilley, G.E., and Fildani, A., 2010, A test of initiation of submarine leveed channels by deposition alone: Journal of Sedimentary Research, v. 80, p. 710–727.

Sheets, B.A., Paola, C.S., and Kelberer, J.M., 2007, Creation and preservation of channel-form sand bodies in an experimental alluvial system, *in* Nichols, G., Williams, E., and Paola, C., eds., Sedimentary Processes, Environments and Basins: A Tribute to Peter Friend, International Association of Sedimentologists, Special Publication 38, p. 555–567.

Shumaker, L.E., Jobe, Z.R., Johnstone, S.A., Pettinga, L.A., Cai, D., and Moody, J.D., 2018, Controls on submarine channel-modifying processes identified through morphometric scaling relationships: Geosphere, v. 14, p. 1–17, doi:10.1130/GES01674.1.

Sprague, A.R., Patterson, P.E., Hill, R.E., Jones, C.R., Campion, K.M., Van Wagoner, J.C., Sullivan, M.D., Larue, D.K., Feldman, H.R., Demko, T.M., Wellner, R.W., and Geslin, J.K., 2002, The physical stratigraphy of fluvial strata: a hierarchical approach to the analysis of genetically related stratigraphic elements for improved reservoir prediction [abstract]: American Association of Petroleum Geologists, Annual Meeting.

Stevenson, C.J., Jackson, C.A.-L., Hodgson, D.M., Hubbard, S.M., and Eggenhuisen, J.T., 2015, Deep-water sediment bypass: Journal of Sedimentary Research, v. 85, p. 1058–1081.

Stevenson, C.J., Feldens, P., Georgiopoulou, A., Schonke, M., Krastel, S., Piper, D.J.W., Lindhorst, K., and Mosher, D., 2018, Reconstructing the sediment concentration of a giant submarine gravity flow: Nature Communications, v. 9, 2616.

Strong, N., and Paola, C., 2008, Valleys that never were: time surfaces versus stratigraphic surfaces: Journal of Sedimentary Research, v. 78, p. 579–593.

Sullivan, M., Jensen, G., Goulding, F., Jennette, D., Foreman, L., and Stern, D., 2000, Architectural analysis of deep-water outcrops: implications for exploration and development of the Diana sub-basin, western Gulf of Mexico, *in* Weimer, P., Slatt, R.M., Coleman, J., Rosen, N.C., Nelson, H., Bouma, A.H., Styzen, M.J., and Lawrence, D.T., eds., Deep-Water Reservoirs of the World: Gulf Coast Section, SEPM, 20th Annual Research Conference, p. 1010–1031.

Sumner, E.J., and Paull, C.K., 2014, Swept away by a turbidity current in Mendocino submarine canyon, California: Geophysical Research Letters, v. 41, 7611–7618.

Sylvester, Z., Pirmez, C., and Cantelli, A., 2011, A model of submarine channel–levee evolution based on channel trajectories: implications for stratigraphic architecture: Marine and Petroleum Geology, v. 28, p. 716–727.

Symons, W.O., Sumner, E.J., Paull, C.K., Cartigny, M.J.B., Xu, J.P., Maier, K.L., Lorenson, T.D., and Talling, P.J., 2017, A new model for turbidity current behavior based on integration of flow monitoring and precision coring in a submarine canyon: Geology, v. 45, p. 367–370.

Talling, P.J., Allin, J., Armitage, D.A., Arnott, R.W.C., Cartigny, M.J.B., Clare, M.A., Felletti, F., Covault, J.A., Girardclos, S., Hansen, E., Hill, P.R., Hiscott, R.N., Hogg, A.J., Clarke, J.H., Jobe, Z.R., Malgesini, G., Mozzato, A., Naruse, H., Parkinson, S., Peel, F.J., Piper, D.J.W., Pope, E., Postma, G., Rowley, P., Sguazzini, A., Stevenson, C.J., Sumner, E.J., Sylvester, Z., Watts, C., and Xu, J., 2015, Key future directions for research on turbidity currents and their deposits: Journal of Sedimentary Research, v. 85, p. 153–169.

Törnqvist, T.E., Wallinga, J., and Busschers, F.S., 2003, Timing of the last sequence boundary in a fluvial setting near the highstand shoreline: insights from optical dating: Geology, v. 31, p. 279–282.

Trabucho-Alexandre, J., 2014, More gaps than shale: erosion of mud and its effect on preserved geochemical and palaeobiological signals, *in* Smith, D.G., Bailey, R.J., Burgess, P.M., and Fraser, A.J., eds., Strata and Time: Probing the Gaps in Our Understanding: Geological Society of London, Special Publication 404, p. 251–270.

Traer, M.M., Fildani, A., Fringer, O., McHargue, T., and Hilley, G.E., 2018, Turbidity current dynamics: 1. Model formulation and identification of flow equalibrium conditions resulting from flow stripping and overspill: Journal of Geophysical Research, Earth Surface, v. 123, p. 501–519.

Vendettuoli, D., Clare, M.A., Hughes Clarke, J.E., Vellinga, A., Hizzet, J., Hage, S., Cartigny, M.J.B., Talling, P.J., Waltham, D., Hubbard, S.M., Stacey, C., and Lintern, D.G., 2019, Daily bathymetric surveys document how stratigraphy is built and its extreme incompleteness in submarine channels: Earth and Planetary Science Letters, v. 515, p. 231–247.

Walker, R.G., 1975, Nested submarine-fan channels in the Capistrano Formation, San Clemente, California: Geological Society of America, Bulletin, v. 86, p. 915–924.

Wheeler, H.E., 1958, Time-Stratigraphy: American Association of Petroleum Geologists, Bulletin, v. 42, p. 1047–1063.

Wheeler, H.E., 1964, Baselevel, lithosphere surface, and time-stratigraphy: Geological Society of America, Bulletin, v. 75, p. 599–610.

Wynn, R.B., Cronin, B.T., and Peakall, J., 2007, Sinuous deep-water channels: genesis, geometry and architecture: Marine and Petroleum Geology, v. 24, p. 341–387.

Xu, J.P., Barry, J.P., and Paull, C.K., 2013, Small-scale turbidity currents in a big submarine canyon: Geology, v. 41, p. 143–146.

Xu, J.P., Sequieros, O.E., and Noble, M.A., 2014, Sediment concentrations, flow conditions, and downstream evolution of two turbidity currents, Monterey Canyon, USA: Deep-Sea Research Part I, v. 89, p. 11–34, doi: 10.1016/j.dsr.2014.04.001.

Received 24 April 2019; accepted 9 January 2020.

Downloaded from http://pubs.geoscienceworld.org/sepm/jsedres/article-pdf/90/7/673/5129451/i1527-1404-90-7-673.pdf
by guest